Propagation of optically generated acoustic phonons in Si

J. A. Shields, M. E. Msall, M. S. Carroll, and J. P. Wolfe
Physics Department and Materials Research Laboratory, University of Illinois at Urbana-Champaign, Urbana, Illinois 61801
(Received 23 April 1992; revised manuscript received 25 January 1993)

This paper deals with the spectral and spatial distributions of nonequilibrium acoustic phonons produced by optical excitation of a high-purity Si crystal at low temperatures ($T < 2$ K). We report the observation of a quasidiffusion process in Si, resulting from anharmonic-decay and elastic-scattering processes. We show that the observation of quasidiffusive propagation was previously masked by the losses of high-frequency phonons into the helium bath. By removing the contact of the helium bath from the excitation surface, we have quantified the effects of the bath on the detected heat pulses. As the power density of the optical pulses is increased, qualitative changes occur in the shapes of the heat pulses, and at high density, the quasidiffusive propagation is bypassed by the emergence of a localized source of low-frequency phonons. The threshold density for the formation of the localized source is far below that calculated for a "hot spot" based on phonon-phonon interactions. We postulate that the photoexcited carriers, largely in the form of electron-hole droplets, are playing a dominant role in determining the frequency distribution of emitted phonons. Our experiments employ a wide variety of techniques to characterize the propagation of nonequilibrium phonons in silicon: Phonon imaging is used to gauge the size and lifetime of the phonon sources, as well as indicate the frequency distribution of the detected phonons. Comparison is made between direct photoexcitation of silicon and optical excitation of a metal film deposited on the silicon surface. These experiments and Monte Carlo simulations give insight into the diffusion of high-frequency phonons near the interface. The occurrence of a helium bubble at a point of high excitation is shown to have a marked influence on the detected heat pulses.

I. INTRODUCTION— HEAT PULSES IN Si AT LOW TEMPERATURES

The propagation of nonequilibrium phonons in nonmetallic crystals at low temperatures involves a variety of physical processes, including anharmonic decay, elastic scattering, phonon-phonon interactions, and electron-phonon interactions.[1] The principal methods used to study these processes are thermal conductivity and heat pulses. The latter approach is particularly attractive because one can distinguish ballistic and diffusive heat propagation by time-of-flight techniques,[2] phonon spectroscopies,[3] and phonon imaging.[4] Despite technological advances in the available tools, some simple questions remain unresolved. In particular, how the frequency and spatial distributions of phonons evolve following a local excitation in the crystal—whether by optical, electronic, or nuclear means—is difficult to calculate and to measure experimentally. This is true even in pure crystalline silicon, where the elastic properties are known quite well.

The principal difficulty lies in determining the scattering rates of phonons in an anisotropic medium. Experiments have recently measured[5] the fundamental rate of *elastic* scattering from atomic isotopes in high-purity Si; however, the intrinsic *inelastic*-scattering processes (e.g., frequency down-conversion rates) have not been directly measured.[6] Also, the behavior of nonequilibrium phonons at high densities—the regime of the so-called "phonon hot spot"—is not well understood. Increasing technological pressures to develop, for example, phonon-based particle detectors[7] have intensified the attention paid to these basic crystalline processes. In the present paper, we concentrate on the propagation of acoustic phonons in silicon under several common excitation and boundary conditions. Some unorthodox experimental measurements are introduced which allow us to answer several vexing problems that have arisen in the literature.

Photoexcitation of crystalline silicon with visible light generates heat as a byproduct of electronic excitation. Photons incident on the crystal initially create electron-hole pairs with kinetic energies equal to the photon energy minus the semiconductor gap. This "excess energy" given to an *e-h* pair is quickly dissipated (in less than a nanosecond) by emission of photons as the carriers relax to their respective band extrema, where their recombination can produce infrared luminescence. These "thermalization" phonons are initially in the form of high-energy optical phonons, which down convert to lower-energy acoustic phonons on a subpicosecond time scale. By virtue of lattice anharmonicities, the resulting acoustic phonons continue to split into lower-frequency acoustic phonons as they propagate in the bulk of the crystal.

In addition, the "thermalized" *e-h* pairs can recombine nonradiatively, producing high-frequency optical and acoustic phonons which add to the shower of nonequilibrium phonons that are the byproduct of photoexcitation. The generation of "recombination" phonons continues until the supply of nonequilibrium carriers is exhausted, which, in indirect-gap semiconductors such as silicon, can be several microseconds. If the instantaneous flux, or thermal energy per area per second, produced by such delayed recombination were less than the initial burst caused by the thermalization phonons, then the principal source of high-frequency acoustic phonons

would have a duration comparable to that of the excitation pulse. However, we present evidence in this work that even at moderate excitation levels, the source lifetimes are rather long, indicating that the photoexcited carriers in Si play a major role in determining the temporal and frequency distributions of the nonequilibrium phonons.

Experimentally, the physical processes involved (e.g., the frequency down conversion and elastic scattering of the optically generated acoustic phonons) are surmised from measurements of the heat pulses detected at some distance from the excitation source, usually at an opposing surface of the crystal. Useful information is contained in the temporal shape of the heat pulses (from times of flight) and the spatial distribution of heat flux (from phonon imaging).

In 1989, Maris[8] pointed out an apparent anomaly in the published phonon images produced by direct photoexcitation of semiconductors such as Ge, Si, and GaAs. The images were much sharper than expected from considering the predicted frequency distribution and scattering rates of optically generated phonons. His reasoning was as follows: high-frequency longitudinal-acoustic phonons produced by the decay of optical phonons are expected to undergo anharmonic decay to low frequency at a rate[9]

$$\tau_a^{-1}=B\nu^5 = \left[\frac{0.074}{\mu\text{s}}\right]\left[\frac{\nu}{\text{THz}}\right]^5 \text{ for Si}, \quad (1)$$

where ν is the frequency of the initial phonon. In addition, the phonons will elastically scatter from randomly appearing isotopes at a rate[10]

$$\tau_e^{-1}=A\nu^4 = \left[\frac{2.43}{\mu\text{s}}\right]\left[\frac{\nu}{\text{THz}}\right]^4 \text{ for Si}. \quad (2)$$

The net result of these two processes is that the phonons undergo "quasidiffusion" (diffusion plus down conversion), as discussed previously by Levinson and others,[11–13] whereby each successive frequency generation has about half the frequency and about $2^{9/2}$ times the diffusion length of the previous generation. That is, the diffusion length of the generation with lifetime τ_a is given by

$$l=(D\tau_a)^{1/2}=(\tfrac{1}{3}V^2\tau_e\tau_a)^{1/2}=\left[\frac{1}{3}\frac{V^2}{AB\nu^9}\right]^{1/2}\sim\nu^{-9/2}, \quad (3)$$

where V is an average phonon velocity. Maris pointed out that the phonons arriving at the detector have originated from the previous generation's diffusive cloud, which should be $2^{9/2}$ (about 23) times smaller than the size of the crystal. The sharpness of the phonon images, on the other hand, indicates that the phonon source is at least an order of magnitude smaller than this.

It is important to realize that a given phonon with frequency ν_0 does not simply decay into two phonons with frequency $\nu_0/2$. The simplest one-branch model of the anharmonic decay of a phonon at ν_0 leads to the collinear production of two daughter phonons, one with ν and the other with $\nu_0-\nu$, with a probability

$$P(\nu_0,\nu)=\frac{\nu^2(\nu_0-\nu)^2}{\nu_0^5} \quad (4)$$

plotted in Fig. 1(a). Figure 1(b) shows that a small subset of the phonons is down converted to a sufficiently low frequency that they can traverse the crystal ballistically, giving rise to sharp phonon-focusing caustics when a near-ballistic time of flight is selected. This simple model predicts that, even for an initial frequency of $\nu_0=3.75$ THz, a significant fraction of the daughter phonons have calculated mean free paths, $V\tau_e$, larger than the crystal thickness.

A further prediction of the quasidiffusion model is that the phonons arriving at the detector should exhibit a broad spread in their times of flight, due to the distribution of path lengths in a diffusion process. (We ignore for the moment the aforementioned phonons which emanate from carrier recombination at delayed times.) Indeed, broad heat pulses were observed in photoexcited GaAs and successfully modeled by a Monte Carlo calculation of the quasidiffusion process.[14] However, as discussed below, reported heat pulses in photoexcited Si are much

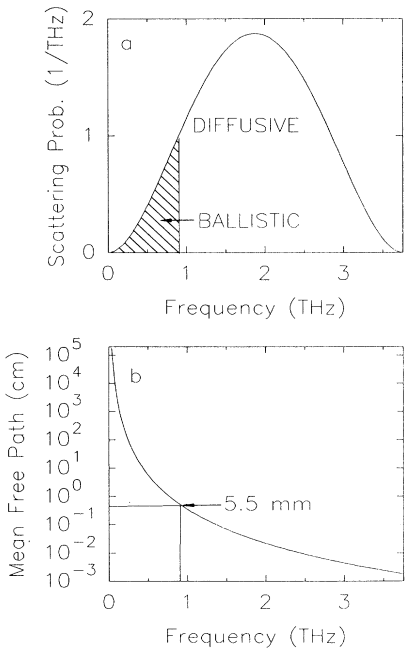

FIG. 1. (a) Distribution of frequencies resulting from a single decay of 3.75-THz phonons [Eq. (4)]. The shaded region indicates those phonons which travel ballistically through a 5.5-mm sample, as indicated by the mean free paths displayed in (b). (b) The mean free path is $V\tau_e$, with $V=8.65$ mm/μs, an average longitudinal phonon velocity and τ_e given by Eq. (2). τ_a in Eq. (1) is longer than τ_e.

shorter than predicted by the quasidiffusion model.

For Si, a Monte Carlo calculation of the quasidiffusive pulse resulting from the above processes is shown in Fig. 2. This calculation by Maris[15] assumes an isotropic crystal 1 cm thickness, mode averaged scattering rates, and a phonon velocity equal to the Debye velocity. The sharp peak at the ballistic time, $t_b \approx 1.7$ μs, is associated with the low-frequency phonons which travel from the source to the detector ballistically (those in the shaded region of Fig. 1). The long tail, with $\tau_{1/e} = 5.75$ μs, is due to the higher-frequency phonons which scatter several times in the crystal. This simple prediction ignores the anisotropies inherent in the propagation and scattering processes, but still provides a strong argument that the majority of photoproduced phonons in Si will not propagate ballistically from source to detector. We expect only a weak component of sharply focused ballistic phonons.

Experiments by Shields and Wolfe,[16] on a 2-cm cube of Si immersed in a helium bath at 2 K, do not bear out these predictions. The observed heat pulses, generated by a tightly focused 10-ns Ar^+ laser beam, display no long tail from scattered phonons, as shown in Fig. 3(a). In addition, the phonon caustics, shown in Fig. 3(b), are very sharp. These observations imply that the detected phonons originate from a region very near the focused laser source: the source spot radius is about 20 μm at low powers, compared to a source dimension of $(2)^{-9/2}(2\text{ cm}) \approx 1$ mm predicted for quasidiffusion. The conclusion drawn from these remarkable results is that frequency down conversion is occurring much more rapidly than given by Eq. (1), resulting in a *localized source of low-frequency phonons.* It was suggested in Ref. 15 that a "phonon hot spot" was formed which acted to thermalize the highly nonequilibrium distribution of phonons. Down conversion of phonons at surface defect and impurity sites may also help thermalize the nonequilibrium distribution, but this effect can be minimized by careful surface preparation.

An additional observation[16] that the size of the phonon source—as determined by the sharpness of the phonon caustics—expands as the excitation power is increased is also inconsistent with the simple quasidiffusion picture, which is independent of excitation density. However, subsequent calculations, which included phonon-phonon interactions, have predicted an increase in source (hot spot) volume with excitation power.[17] Despite experimental efforts at the time, lowering the power level did not result in a vanishing of the localized source; no fuzzing of the image or broadening of the heat pulses were observed even at low powers. Indeed, the caustics were sharpest at the lowest observable excitation level.

In this paper we describe a set of experiments which begin to resolve the dramatic contrasts between expectation and observation. The present experiments encompass a much broader range of excitation densities and examine the effects of liquid helium at the excitation surface. To provide necessary perspective, we also examine the case where the heat source is an optically excited metal film on the crystal surface. Imaging techniques are

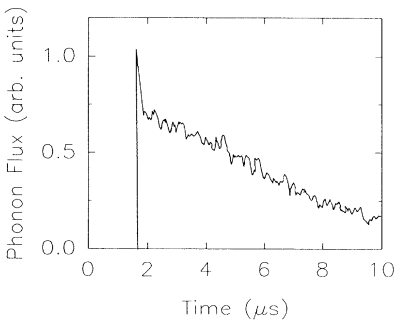

FIG. 2. Calculated time trace for quasidiffusive propagation through a 1-cm silicon sample, after Maris, Ref. 15.

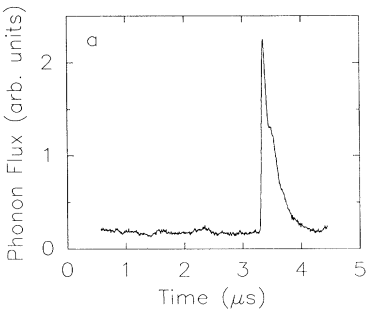

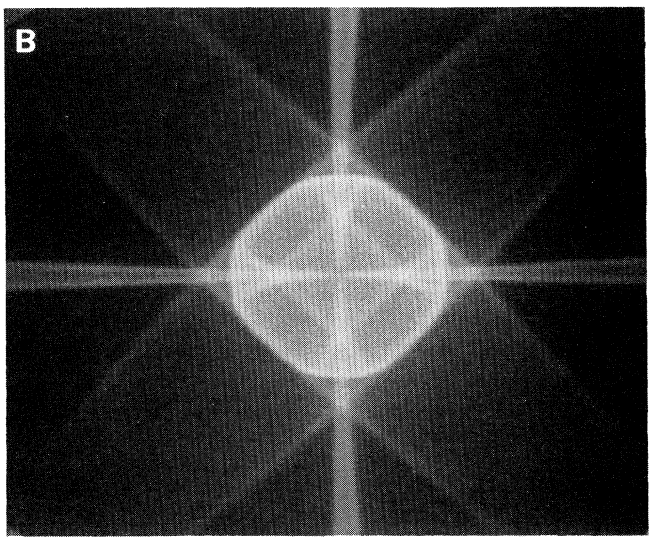

FIG. 3. (a) Intensity of the phonon signal vs time in photoexcited silicon at $T = 1.8$ K. The propagation direction is along a slow transverse (ST) caustic which is 7° from [001] in the 010 horizontal plane. The onset of the ballistic signal at $t = 3.2$ μs indicates significant ST ballistic signal. The longitudinal pulse is not observed due to phonon focusing. The central caustic structure is referred to as the "ST box" (Ref. 16). (b) High-resolution phonon image of silicon with direct photoexcitation. The center of the image corresponds to the [001] propagation direction. The width of the image is about 43° left to right.

employed which provide information about the evolution of the phonon frequencies and spatial distributions as well as isolate the ballistic and scattered phonons. The study requires practical applications of angular dispersion effects and "spatial filtering," introduced in earlier work. We find several unexpected results. For example, it now seems unlikely that phonon-phonon interactions are the cause of the localized phonon source in photoexcited silicon. We also find that the presence of liquid helium at the boundary has dramatic effects on the heat pulses. We have formed a hypothesis about the phonon source in Si: a variety of indirect evidence suggests that the photoexcited carriers—probably in the form of electron-hole droplets—play an important role in the rapid creation of low-frequency phonons. Further experiments are proposed which could verify this hypothesis.

II. DIRECT PHOTOEXCITATION (DP)—EXPERIMENTAL RESULTS

The experiments described in this paper are performed on a $5.5\times6\times10$ mm^3 [100]-oriented silicon crystal. The crystal was mechanically polished with a 0.1-μm alumina suspension and chemically etched with Syton (a standard preparation) to remove subsurface damage. Qualitatively similar results have also been obtained in experiments on a 2.75-mm-thick [100]-oriented Si crystal. The detector is a 6×30-μm^2 granular aluminum bolometer sputter deposited on the 6×10-mm^2 [100] sample face in an argon-oxygen atmosphere. The sample is immersed in a liquid-helium bath at 1.7 K, the transition temperature of the aluminum oxide bolometer film. The time response of the detector is measured by directly exciting the detector film with a low-intensity laser pulse. The full width at half maximum (FWHM) response to a 10-ns laser pulse was 85 ns for the first direct-photoexcitation experiments, but deteriorated to 110 ns for some of the later metal-film experiments because of the thermal cycling. Minimum laser spot size (FWHM) is 20 μm.

Our experiments have shown that the presence of liquid helium at the excitation surface has dramatic effects on the heat pulses. To eliminate this effect we seal a transparent "window" against the excitation surface of the sample with a ring of soft indium metal. This is done at room temperature with the sample and window located in a nitrogen atmosphere. When the sample is cooled to helium temperatures, the nitrogen gas condenses into a solid film on the surfaces within the sealed region, leaving a cryopumped vacuum adjacent to the excitation surface. We denote this condition with the term "isolated surface," indicating that we have isolated the surface from the helium bath. The other surfaces of the sample, including the detector surface, are contacting a superfluid liquid-helium bath. For direct comparison to the case of a "helium" interface, the indium seal may be broken, leaving all other conditions the same. This necessitates warming the sample, but we have found that the bolometer detector described above is stable for a number of temperature cycles.

It is reasonable to expect that the shapes of the heat pulses generated near a crystal surface depend to some extent on the boundary conditions at that surface. The reflectivity of phonons at an interface depends on the acoustic properties of the contacting materials as well as the quality of the interface. Typical phonon imaging experiments on Si, such as those described in Fig. 3, are conducted with a polished crystal immersed in superfluid helium. Despite the large acoustic mismatch between Si and ^{4}He, it is well known that crystalline phonons incident on such a surface have about a 50% chance of being transmitted into the liquid helium—an effect known as the anomalous Kapitza conductance.[18] The loss of phonons into the helium can certainly affect both the heat flux propagating into the bulk of the crystal and the threshold for creating a (hypothetical) hot spot at the excited surface. Also, at high excitation densities, it is known that the liquid helium is locally vaporized at the excitation point, creating a gas bubble which may further modify the boundary conditions.

The effect of removing the liquid helium from the excitation surface is striking. Figure 4 shows the heat-pulse signal generated by a *defocused* 10-ns laser pulse of approximately $P=0.5$ W peak power absorbed in the sample. A measured beam diameter of 1.0 mm implies a very low power density. This combination of an isolated excitation surface and low power density produces a heat pulse which is remarkably similar to the Monte Carlo predictions of Fig. 2. For our 5.5-mm-thick crystal, the measured $1/e$ decay time of the tail is 4.5 μs, which compares favorably to the 5.75 μs characterizing Maris's isotropic calculation for a 1-cm-thick sample. *This is one of the most important results of our work, showing that the*

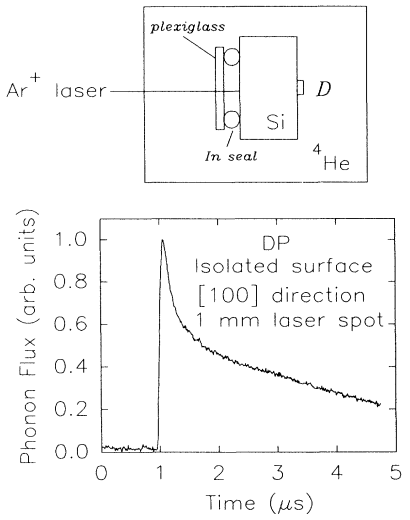

FIG. 4. Experimental time trace showing quasidiffusion in a 5.5-mm silicon sample under direct photoexcitation (DP) by a defocused argon-ion laser ($P/A=0.59$ W/mm^2). The excitation surface is isolated by cryopumped vacuum, as illustrated in the schematic above. A Plexiglas window is sealed directly on the sample surface with indium in a nitrogen atmosphere at room temperature. When the apparatus is immersed in superfluid helium the space between the window and the sample cryopumps to very low pressure.

quasidiffusive propagation via anharmonic and elastic scattering processes is a relevant description of phonon propagation in weakly photoexcited Si. We see that the heat pulse is composed of a sharp component at the ballistic time of flight (corresponding to a small number of low-frequency phonons) followed by a long tail of heat flux (corresponding to the diffusive propagation of higher-frequency phonons with shorter mean free path). The intensity of the ballistic spike depends on the method of isolating the excitation surface. Subsequent experiments using an evacuated chamber show a less prominent ballistic spike, suggesting that this feature is affected by a surface film.

The relative amplitudes of the ballistic and diffusive components depend somewhat on the direction of propagation chosen. In the experiment of Fig. 4, the laser beam is centered on the "ST box" (where ST denotes slow transverse) shown in Fig. 3(b) and the excitation covers a fair portion of the box area. In Fig. 5, we show an expanded time trace of the heat pulse obtained at relatively low power density, plotted both linearly and logarithmically. The log plot reveals an approximately exponential decay between 2.5 and 10 μs.

Figure 6(a) shows what happens when liquid helium is in contact with the excitation surface. A dramatic reduction in the diffusive tail is observed. We conclude that a large fraction of the high-frequency phonons are lost into the helium bath. These diffusing phonons have a high probability of intersecting the sample surface, where they have a significant probability of transmission into the bath.

Figures 6(b) and 6(c) show the effects of raising the excitation density by focusing the laser beam. At high excitation densities the long quasidiffusive tail on the heat pulse is much reduced for all excitation conditions, indicating a great reduction in the relative number of high-frequency phonons emitted from the source region. We have repeated this experiment using a mechanically pumped vacuum chamber to isolate the excitation surface [denoted as the "vacuum" interface condition and shown in Fig. 6(c)] and see sharp pulses in both cases of focused

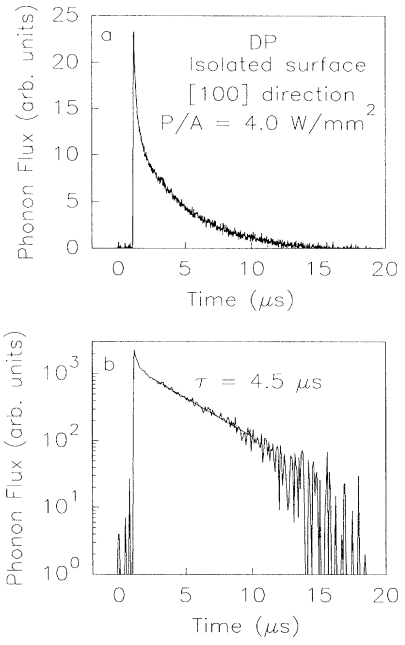

FIG. 5. Experimental time trace showing quasidiffusion for (a) linear and (b) log plots. The tail of the pulse is approximately exponential with the time constant shown.

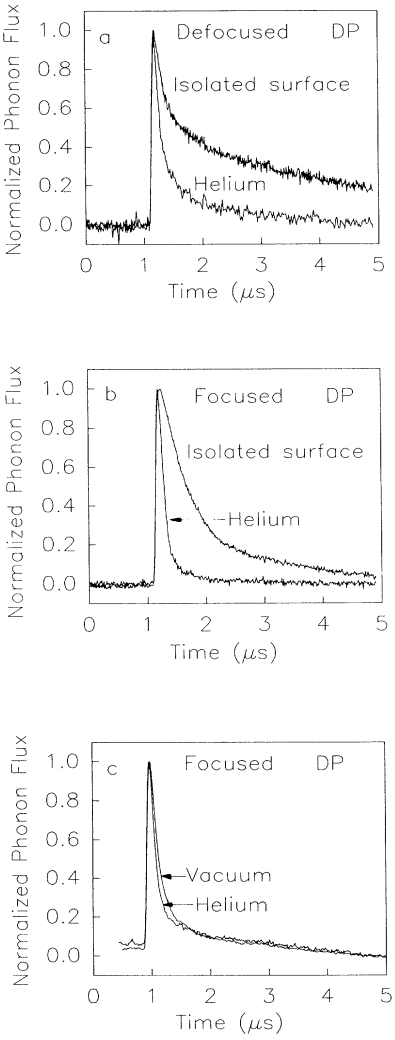

FIG. 6. A comparison of time traces for the DP defocusing experiment, with and without the excitation surface in contact with liquid helium. All of these traces are normalized to the same peak height. Typically a factor of 3–7 reduction in the peak height is observed when liquid helium is in contact with the excitation surface. (a) Low power density comparison between helium and "isolated surface" data. At these low excitation levels a helium bubble does not form. (b) At high power density, the heat pulses change character. In the helium case a small helium bubble is formed at the excitation point and a long-lived source is observed in the isolated surface case. Both these results are discussed in detail in Sec. VI. (c) At high power density, the mechanically pumped vacuum case and the helium case show the same pulse shape, indicating that a low-frequency phonon source is present.

excitation. (As indicated above, with defocused excitation the "vacuum" condition largely reproduces the isolated surface results shown in Fig. 4, except that the ballistic spike is reduced.) We attribute the differences between the high excitation "vacuum" and isolated surface conditions in Figs. 6(b) and 6(c) to the cryopumped film on the isolated surface, although the detailed mechanism is unknown.

In order to evaluate the effect of phonon losses into the helium bath, a Monte Carlo calculation which simulates the experimental conditions has been performed. In this program, a random array of 4-THz phonons introduced at a point on the sample surface is allowed to decay and elastically scatter according to the rates for longitudinal phonons given by Eqs. (1) and (2). A histogram of the times of arrival is collected at a given radius from the excitation point. The "vacuum" case assumes 100% specular reflection from the surface, and the "helium" case assumes a 50% loss rate into the helium with each incidence at the surface. Figure 7(a) shows the remarkable effectiveness of the helium in absorbing the high-frequency diffusive phonons, which is in qualitative agreement with the data of Fig. 6(a).

A tabulation of the frequencies of the phonons which are lost into the helium in this simple model is given in Fig. 7(b). The frequency distribution of lost phonons closely mimics that of the first generation of phonons down converted from $\nu_0=4$ THz, given by Eq. (4) and shown as the broad curve in Fig. 7(b). Not shown in Fig. 7(b) is a large spike of several thousand 4-THz phonons ($\approx 58\%$ of the initial number) which are also lost into the helium. Thus most of the phonons lost into the helium bath are either original 4-THz phonons or their daughters. The frequency distribution of the detected phonons (i.e., those not lost into the helium) resembles the distribution of Eq. (4) with $\nu_0 \approx 2$ THz [lower solid curve in Fig. 7(b)], representing the second generation phonons. Figure 7(c) shows that the *detected* frequency distribution is only slightly altered by the presence of helium at the excitation surface because high-frequency phonons generally undergo two or more down-conversion events before reaching the detector.

Let us now consider more closely the effects of raising the power density in the vacuum-interface experiment.[19] The schematic diagram in Fig. 8 shows how we change the power density over a wide range *without* changing the peak power incident on the sample. The combination of two lenses allows for a smaller minimum spot size than is

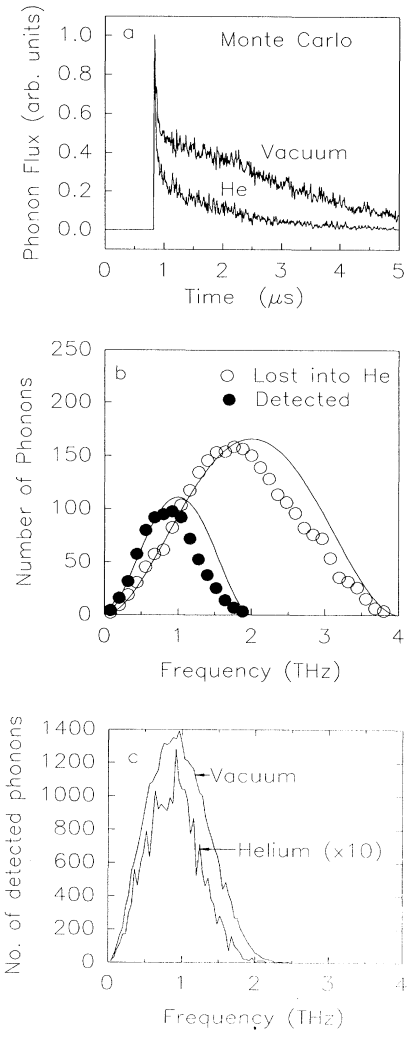

FIG. 7. (a) Isotropic calculation of time traces for phonon propagation through a 5.5-mm-thick Si sample in vacuum or in helium bath. The bath absorbs a large fraction of the diffusive phonons which comprise the long tail in the vacuum trace, so that the helium trace is mainly a sharp ballistic pulse. (b) Calculated frequency distribution of detected phonons for both cases.

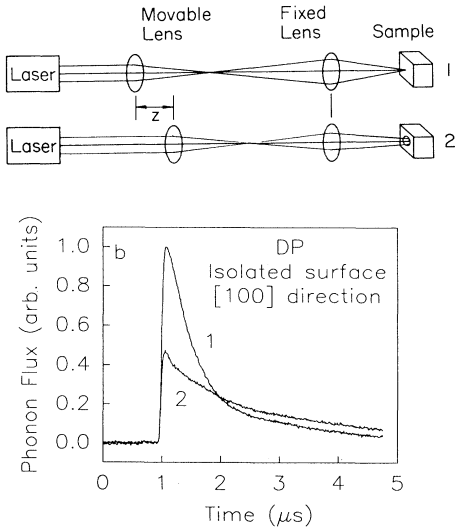

FIG. 8. (a) Schematic diagram of the optical apparatus used to vary the excitation power density without changing the total incident power. (b) Effect of defocusing on the shape of the time traces under isolated surface excitation. Curve 1: high excitation density; curve 2: low excitation density.

attainable with a single lens due to the spatial restrictions of the cryostat (not shown). The spot size is determined by measuring the sharpness of a target pattern placed at the excitation surface. The excitation area is taken as $|\pi/4| \times (\text{FWHM})^2$, in terms of the full width at half maximum of the beam profile. The minimum spot size measurement could be in error by as much as a factor of 2. The power density is defined as the peak instantaneous absorbed laser power divided by the excitation area. To minimize the effects of phonon focusing when changing the focal area, we center the laser beam on the [100] axis [center of Fig. 3(b)] and adjust the alignment of the beam so that there is no lateral translation of the spot as the focusing lens is translated along the beam axis. The size of the laser beam on the sample is always less than 1 mm, which kept the excitation region within the "ST box."

The data in Fig. 8 reveal interesting changes in the heat-pulse intensity and shape as the power density is increased. At the highest levels, a large increase in the peak phonon flux is observed accompanied by a decrease in the tail intensity. The average arrival time becomes closer to the ballistic time of flight and the integrated intensity appears to increase, despite the fact that the total absorbed laser power changes very little. This increase in the near-ballistic signals is not due to phonon-focusing effects because the excitation area is kept within a relatively flat intensity region of the ST box, as verified in metal-film-excitation experiments described below.

What is the cause of the sharper, more intense heat pulse at high excitation density? It may be an indicator of the onset of a phonon hot spot, or it may indicate the onset of a new regime of phonon-carrier interactions. We can characterize the effect by plotting the intensities of the peak and the tail as a function of power density. The data for several different peak-power levels are plotted in Fig. 9. The signals for different powers are normalized to the same peak height at low power densities. We see that the peak-height curves lie along a universal curve, with lower and upper intensities differing by a factor of about 3 and a well-defined transition region which is best defined by power density rather than peak power or excitation area. The change in the tail heights, which decrease with increasing power density, is both smaller and less abrupt than that observed for the peak height. (These results are qualitatively the same for both isolated surface and "vacuum" excitation conditions.)

The extra phonons (those arriving mainly between 1.0 and 1.5 times the ballistic time) observed at high power densities give rise to a sharp caustic pattern, just as in the previous helium experiments of Shields and Wolfe.[16] Therefore this new component in the heat pulse (distinct from the quasidiffusive tail) arises from a *localized* source which predominantly emits phonons of sufficiently low frequency to transit the crystal ballistically.

The lifetime of this localized phonon source can be measured by a "spatial filtering" technique, first used by Greenstein, Tamor, and Wolfe[20] in Ge. Time traces are recorded with the focused laser beam on and off a sharp caustic, and these two traces are subtracted, as shown in Fig. 10(a). Because the two laser positions are close together, the delocalized, or scattered, part of the heat flux should be nearly identical. *The "difference trace," therefore, records the time evolution of the localized source.* We see in Fig. 10(a) that the long tail is indeed removed by this subtraction. The semilogarithmic plot of Fig. 10(b)

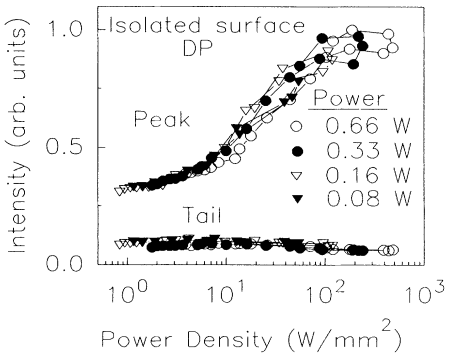

FIG. 9. Peak heights (t near 1.1 μs in Fig. 8) and tail heights (averaged between $2.75 < t < 3.25$ μs) as a function of power density for four different total powers. For a given peak power P, the power densities are varied continuously by changing the excitation area, as indicated in Fig. 8(a). The intensities of the peak heights at different total powers are scaled to be equal at the lowest power density for ease of comparison. A transition in the character of the heat pulse occurs at a power density of about 20 W/mm^2.

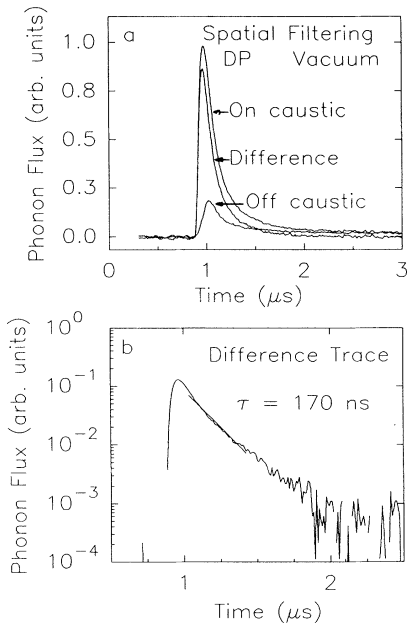

FIG. 10. Measurement of source lifetime using spatial filtering. (a) Subtracting the off-caustic time trace from the on-caustic trace yields a purely ballistic difference trace. (b) The difference trace plotted on a semilogarithmic scale shows that the decay of the source is roughly exponential over two orders of magnitude with a decay time of about 170 ns. The remaining signal at late times may be due to incomplete subtraction of the bulk scattering. The total power is 100 mW, with a laser spot size of 40 μm (FWHM).

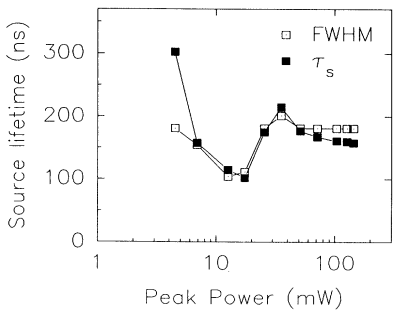

FIG. 11. The measured lifetime of the localized source, τ_s, as a function of absorbed power. Also plotted are the full width at half maximum of the spatially filtered heat pulses which are comparable to the decay times. These data show the onset of a source of (low-frequency) ballistic phonons at peak powers greater than about 30 mW, in rough agreement [power density is equal to 30 mW/($\pi\times400$ μm^2)=15 W/mm^2] with the thresholds seen in Fig. 9. The lowest power levels probably correspond to quasidiffusive propagation with a large effective source size, so the interpretation of these spatially filtered data is not straightforward.

shows that, at this power level, the measured decay time is 170±30 ns. By deconvolving the detector response of 64 ns, we extract the lifetime of the localized source, $\tau_s=(170^2-64^2)^{1/2}=157\pm25$ ns.

In order to employ the spatial filtering method for measuring the source lifetime as a function of excitation level, we are not allowed the luxury of simply defocusing the laser, because a sharp caustic is needed for spatial selection. Instead we lower the excitation level, increase the averaging time, and attempt to reach the power-density threshold for the formation of the localized source. The result of this experiment is shown in Fig. 11. Above 40 mW peak power, the source lifetime appears stable at about 160 ns. Qualitative changes are observed in the difference traces as the power is lowered below 40 mW, indicating a threshold for the onset of the localized phonon source. Could this be the elusive hot-spot threshold predicted by Levinson *et al.*? In order to evaluate this possibility we must compare these threshold densities to those required to form a phonon hot spot.

III. THEORETICAL ESTIMATE OF THE HOT-SPOT THRESHOLD IN Si

The phonon hot spot was originally postulated by Hensel and Dynes[21] to explain a long-lived phonon source which drives the photoexcited electron-hole droplets in Ge. Subsequent experiments by Greenstein, Tamor, and Wolfe[20] indicated that the lifetime of the localized source is 0.1–1.5 μs, depending on excitation power. However, those experiments typically used pulse energies and pulse lengths much larger than in the present experiments (typically, 10 μJ and 100 ns vs 10 nJ and 15 ns in the present work). Theoretical calculations of the phonon hot spot in semiconductors have been published by Levinson and coworkers.[22,23]

The basic idea of a phonon hot spot is that for sufficient densities of nonequilibrium phonons, phonon-phonon scattering will limit the mean free path of the average phonon. Above a certain threshold, the phonons will be localized, establishing a local temperature well above that of the cold crystal. The expected formation threshold occurs when the occupation number of the phonon modes for a typical phonon frequency reaches unity. At this phonon density, up-conversion and down-conversion processes occur at comparable rates and a hot-spot temperature is established.

We wish to know if the transition region occurring at about 20 W/mm^2 in Fig. 9 corresponds to the predicted threshold for hot-spot formation. For a peak absorbed power of 0.33 W this power density corresponds to an excitation area of about 1.7×10^{-4} cm^2=(128 μm)^2 and an energy of 3.3 nJ for the 10-ns pulse. The absorption depth of the laser light is about 1 μm in Si. Approximately half of this energy will be converted to phonons in the initial thermalization process of the photoexcited carriers.

The average frequency of the phonons during a 10-ns excitation pulse can be estimated by setting τ_a equal to 10 ns in Eq. (1), yielding $\nu=4.2$ THz for Si. From Eq. (2), the isotope scattering time for phonons with this frequency is 1.3 ns, which, using Eq. (3), implies that these phonons have diffused an average distance of 12 μm within the 10-ns excitation pulse. The volume occupied by the 4.2-THz phonons is therefore $V=(1.7\times10^{-4}$ cm$^2)(12\times10^{-4}$ cm$)=2\times10^{-7}$ cm^3, yielding a thermal energy density at the end of the pulse of 0.8×10^{-2} J/cm^3.

We must compare this estimate to the energy density required to establish a temperature in the thermally excited volume V. For the predominant phonons to have an occupation number of about 1, the average thermal energy per unit cell, $V_u=(0.34$ nm$)^3$, of the Si crystal must be about $h\nu$ for the 4.2-THz phonons. Thus the predicted energy density threshold for the formation of a hot spot with the given pulse length is $h\nu/V_u=72$ J/cm^3. Thus the hot-spot threshold calculated by this simple estimate exceeds by a factor of 9000 the thermal density calculated above for the experimental pulse. We conclude that under these conditions there is insufficient energy to establish a phonon hot spot in the sense envisioned by Levinson and co-workers.

What then is the source of the dramatic changes in the heat pulses which appears above these relatively low excitation levels? We postulate that the photoexcited carriers are having a significant effect on the acoustic-phonon distribution. Energetic carriers are the original source of phonons, but the daughter phonons are also able to interact with the relaxed carriers. Also, as mentioned at the outset of this paper, phonons are produced by the carrier-recombination process. It is known that at moderate excitation densities, electron-hole droplets are formed in silicon below $T_c=22$ K. The interaction of phonons with droplets will be considered in Sec. VII.

IV. DISCUSSION OF A METAL-FILM RADIATOR

To gain a basis for comparison, we now examine the behavior of heat pulses produced by a "Planckian"

source rather than hot photoexcited carriers. Instead of exciting the crystal directly, we excite a metal film which has been evaporated onto the surface of the crystal. Again, the photons excite carriers, but the strong electron-phonon interaction in the metal is a much more effective relaxer of phonons than the semiconductor. The contrasts between metal-film (MF) excitation and direct photoexcitation will provide insight for understanding the phonon source characteristics.

A. Ballistic phonon transmission resulting from a Planckian source

Phonons generated by photoexcitation of a metal film evaporated on the sample surface are transferred to the sample. Previous studies[24,25] with Ohmically heated films have indicated that the thermal phonon radiation can be modeled by a Planck distribution, in analogy to photon blackbody radiation. By increasing the excitation power the Planck distribution in the film is shifted to higher frequencies. Of course, transmission of phonons across the metal/crystal interface is dependent upon the elastic properties of the two media, in particular, the phonon densities of states. The simplest model for transmission across the interface uses continuum acoustics and is called the acoustic-mismatch (AM) model.

B. Estimates of film temperature and source lifetime

Instantaneous pulsed excitation assumes that a total energy E from the laser pulse is deposited in the metal film before thermal diffusion occurs. The temperature of this volume can then be found using the low-temperature form of the lattice specific heat, i.e.,

$$T^4=\frac{4E}{\rho\alpha V} , \tag{5}$$

where ρ is the density, V is the excited volume, and α is the specific heat constant. In our experiments a 2000-Å copper film evaporated on the silicon crystal is used as the thermal radiator ($\alpha=0.746\times10^{-6}\ \mathrm{J\,g^{-1}\,K^{-4}}$). For a cylindrical deposition volume with a 5-μm radius and 2000 Å depth, the heating from an instantaneous pulse of 10 nJ results in a temperature of 140 K.

Of course, the actual heating of the film is not instantaneous. For a nonzero pulse length the resultant temperature will be affected by radiative losses into the crystal and the bath. For the 10–15-ns pulses in our experiments, we assume that a steady-state condition is reached at each instant of the excitation pulse, i.e., the thermal relaxation time of the film is shorter than the pulse width (an assumption to be justified below). Following the development of Weis,[25] we employ the acoustic-mismatch model for phonon transmission through interfaces. For phonons the Stefan-Boltzmann law is

$$\frac{P(T)}{A}=\sigma T^4=\frac{\pi^5k^4}{15h^3}\left[\frac{e_L}{c_L^2}+\frac{e_{\mathrm{FT}}}{c_{\mathrm{FT}}^2}+\frac{e_{\mathrm{ST}}}{c_{\mathrm{ST}}^2}\right]T^4 , \tag{6}$$

where $P(T)$ is the instantaneous radiated power, A is the surface area of the excited volume, the c's are phonon velocities in the substrate, FT denotes fast transverse and the e's are the spectral emissivities between the substrate and the radiator.

The calculated values, according to Weis, for the Cu/Si interface in the isotropic limit are $e_L=0.230$ and $e_{\mathrm{FT}}=e_{\mathrm{ST}}=0.152$. For the Cu/He interface we take $e_L=e_{\mathrm{FT}}=e_{\mathrm{ST}}=0.4$, due to the anomalous Kapitza conductance. The resulting values are $\sigma_{\mathrm{Cu/Si}}=174$ and $\sigma_{\mathrm{Cu/He}}=446\ \mathrm{W/m^2\,K^4}$.

Now, in the steady state, energy flux must be conserved so that, for an absorbed laser power P and excitation area A,

$$\frac{P}{A}=\sigma_{\mathrm{Cu/Si}}T^4+\sigma_{\mathrm{Cu/He}}T^4 , \tag{7}$$

yielding the source temperature,

$$T^4=\frac{P}{(\sigma_{\mathrm{Cu/Si}}+\sigma_{\mathrm{Cu/He}})A} . \tag{8}$$

For the cylindrical deposition volume discussed above (5 μm radius, 2000 Å depth) and an excitation power of 1 W, we find a copper-film temperature of 67 K with a helium boundary and 93 K for a vacuum boundary [$\sigma_{\mathrm{Cu/He}}$ set equal to zero in Eq. (8)]. The relaxation time of the radiating film can be found from the rate equation

$$\frac{dE}{dt}=-(\sigma_{\mathrm{Cu/Si}}+\sigma_{\mathrm{Cu/He}})AT^4 . \tag{9}$$

Making use of Eq. (5), we can write

$$\frac{dT^4}{dt}=\frac{-4T^4(\sigma_{\mathrm{Cu/Si}}+\sigma_{\mathrm{Cu/He}})A}{\rho\alpha V}=-\frac{T^4}{\tau} . \tag{10}$$

Thus T^4 decays exponentially with a lifetime τ defined in the above equation. For the conditions stated above, we calculate $\tau_{\mathrm{Cu}}=0.54$ ns when the excitation surface is in a helium bath, and $\tau_{\mathrm{Cu}}=1.9$ ns when the excitation surface is in vacuum. These values are all much shorter than our laser pulse lengths of 10–15 ns, validating the steady-state assumption made above.

It is essential to consider what proportion of a Planckian source of phonons is transmitted through the sample ballistically. Ballistic phonons, which arrive at the detector without scattering, are predominantly low-frequency phonons because the elastic-scattering rate from isotopic defects varies as a fourth power of frequency [Eq. (2)]. The dashed line in Fig. 12(a) shows the predicted transmission factor through a 5.5-mm-thick sample of Si due to this effect. The solid curves are Planck distributions for some representative temperatures normalized to the same total energy. If the excitation area is decreased at a given total excitation energy (as in the defocusing experiment), the temperature of the Planckian phonon source should rise, causing the ballistic component of the detected phonon signal to decrease while the diffusive tail increases. Figure 12(b) shows the resulting ballistic phonon flux transmitted through a 5.5-mm-thick Si sample from the Planck distributions in Fig. 12(a). Thus, in principle, the observed ratio of ballistic to scattered flux at varying excitation densities is an indication of the temperature of a Planckian source.

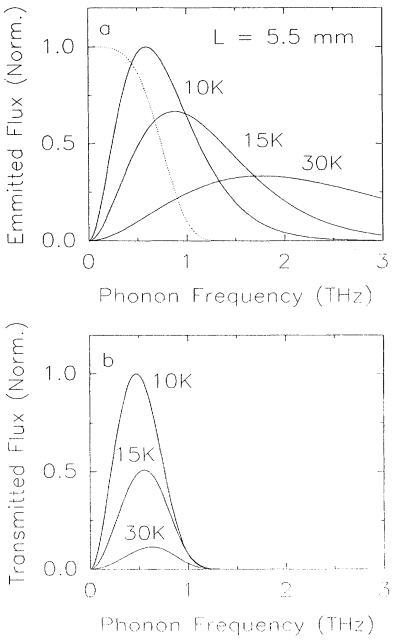

FIG. 12. (a) Planck frequency distributions for the emitted phonon flux, normalized to the same total energy for three different temperatures (solid lines) and the isotope scattering transmission factor (dotted line). (b) The product of the normalized Planck distribution and the transmission factor is the transmitted ballistic energy. Notice that the peak frequency of the transmitted distribution is insensitive to changes in source temperature. The area under the transmitted curve is proportional to phonon signal. (See also Fig. 14.)

V. METAL-FILM EXPERIMENTS

Previous experiments[16] on Si immersed in a He bath had not shown any large differences between the phonon source characteristics of the direct photoexcited case and those with a metal film. This is a surprising result in view of the vast difference in the two experiments, namely, photoexcitation of a metal instead of a semiconductor and an additional interface in the MF experiment. Our present experiments uncover significant differences between DP and MF excitation *when the excitation surface is not in contact with liquid helium.* In part, differences are detectable because the defocusing technique allows us to characterize the source at much lower power densities than those obtainable with focused excitation. (Figure 12 shows that at metal-film temperatures below about 5 K there are essentially no scattered phonons, in contrast to the quasidiffusion observed with DP at low powers). Just as important, however, is the lack of surface losses when the excitation surface is sealed to the mechanically pumped vacuum (as is the case in all the MF data labeled "vacuum"). As described in Sec. II, the isolated surface experiment permitted us to observe the hitherto undetected quasidiffusive signal for the direct photoexcited source; consequently, it is in the MF-vacuum experiments that the differences in heat pulses of DP and MF experiments are most pronounced.

A. Vacuum interface

At first glance, there is nothing surprising about the MF-vacuum heat pulses [Fig. 13(a)]. The ballistic pulses are sharp and there are relatively few phonons in the scattered tail, as expected for a low-temperature metal-film source. However, at the highest excitation densities, where the film temperature estimated by the analysis of the previous section exceeds 30 K, quasidiffusion is not observed. Nor is there a pronounced "long-lived source" similar to that emerging in Fig. 8(b). Figure 13(b) shows that, with a MF-vacuum interface, the ballistic signal intensity decreases and the tail signal increases as the power density is increased, in stark contrast to the DP results in Fig. 9.

From the measured laser spot size we can estimate the temperature of the source region using Eq. (8). From such an estimate, we expect the source temperature to change from 35 to 7 K as the laser is defocused. Figure 14 shows that over this temperature range, the ballistic peak is attenuated by a factor of 2.3. The estimated portions of a Planck distribution which would cross a 5.5-mm sample ballistically (Fig. 12) have a much greater attenuation (≈ 10), as indicated by the trace labeled "no de-

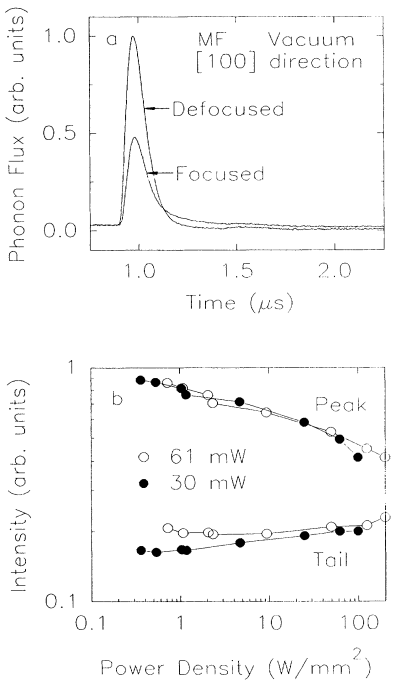

FIG. 13. (a) A comparison of time traces for the metal-film (MF) defocusing experiment, with the excitation surface in mechanically pumped vacuum. As in Fig. 8, the power incident on the sample is constant but the power density is varied by changing the laser spot size. Notice that the effect for MF excitation is *opposite* that for DP, shown in Fig. 8. (b) Peak height ($t \approx 1.1$ μs) and tail height (averaged over $1.3 < t < 1.35$ μs) as a function of power density. The intensities of the peak heights are scaled to be equal to lowest power density. Contrast these results with the DP results in Fig. 9.

cay" in Fig. 14. This estimate is also not compatible with the lack of long tails in the experimental time traces which indicate that the nonballistic signal is a very small percentage of the total signal.

The discrepancy between prediction and experiment can be linked to rapid anharmonic decay of high-frequency phonons in the Si. Simply put, the proportion of experimentally detected phonons is enhanced by contributions from phonons produced by very rapid anharmonic decay of high-frequency phonons in the Si. In this case, the excited region of the metal film does emit a large fraction of high-frequency phonons at high powers, but a fraction of these phonons decay very rapidly to lower frequencies. Low-frequency decay products produced within a few nanoseconds of the conclusion of the laser pulse will be experimentally indistinguishable from low-frequency phonons emitted by the Planckian spot. Figure 14 also includes the results of a Monte Carlo simulation of this process (the trace labeled "with decay"). As the source temperature varies from 7 to 35 K, the simulated ballistic flux changes by a factor of 3, in reasonable agreement with the experimental factor of 2.1. The remaining small discrepancy between experiment and theory could be the result of another down-conversion process: High-frequency phonons which diffuse back to a cold portion of the metal film may be absorbed and quickly down converted in the metal, or simply down converted at defect sites at the metal crystal interface, and reemitted as low-frequency phonons. A Monte Carlo calculation including this effect (not shown) does indeed show a significant lowering of the heat-pulse tail.

B. Helium interface

When liquid helium is in contact with the metallized excitation surface, some remarkable changes occur. Figure 15 shows the results of the defocusing experiment with a helium-MF interface. As the power density is increased, a pronounced tail appears [Fig. 15(a)], but the height of the ballistic peak does not show a significant decrease, unlike the vacuum case in Fig. 13(a). Mysteriously, the integrated intensity increases by a factor of 3 at high power density despite the total power being held constant [Figs. 15(b) and 15(c)].

This large change in integrated intensity is most likely caused by a change in the surface conditions; namely, the formation of a bubble in the helium at the excitation surface. A bubble is formed when thermal losses into the

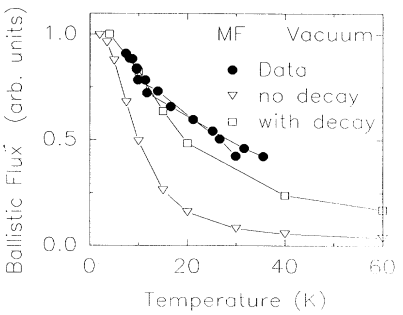

FIG. 14. Ballistic signal intensity as a function of temperature (MF excitation), compared to the expected ballistic signal from a given temperature Planck distribution at these temperatures ("no decay" curve). The curve marked "with decay" is the result of a Monte Carlo calculation of the effect of anharmonic decay and isotope scattering on the detected ballistic signal from a Planck distribution. The intensity of the experimental peaks is scaled to agree with the calculated value at high temperature.

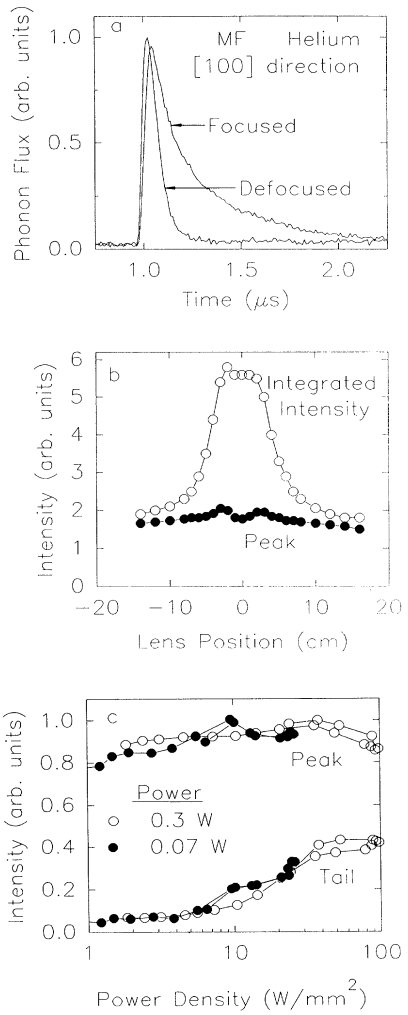

FIG. 15. (a) A comparison of time traces for the MF defocusing experiment, with the excitation surface contacting liquid He. As in previous figures, the power incident on the sample is constant, but the power density is changed. (b) Integrated intensity and peak height of the time traces as a function of lens position (0 cm corresponds to the most tightly focused spot), showing a dramatic increase in integrated intensity. This increase is associated with the formation of a vapor bubble at the excitation surface. (c) Peak height ($t \approx 1.1$ μs) and tail height (averaged over $1.1 < t < 1.3$ μs) as a function of power density. The intensities of the peak heights are scaled to be equal at lowest power density for ease of comparison.

helium are large enough to vaporize the helium near the phonon source. Once this bubble forms, phonon radiation into the helium is less efficient, and the integrated amplitude increases sharply. It is argued below that the bubble also slows the cooling of the film, leading to the extended tail in the focused data of Fig. 15(a), which will be discussed in detail below.

The relative constancy of the ballistic signal when the power density is changed seems to result from a cancellation of two different effects: (a) the decrease expected with a higher-temperature source at constant total power, and (b) an increase expected when the bubble formation causes a reduction in phonon losses into the liquid.

The long tail on the He-MF time trace is evidence that the decay of the phonon signal is slower when the excitation surface is in the helium bath rather than in vacuum. [Fig. 13(a)]. This contradicts intuition which would expect the metal film to cool more quickly when helium is present. Instead the experimental data indicate that the He-MF source pumps energy in the helium bubble which is reradiated into the sample on a longer time scale (or, equivalently, prevents the rapid cooling of the excited metal film). One way to examine what is happening to the source over time is to use the high spatial resolution of the experimental images. *Since phonon dispersion changes the positions of the caustics, measurements of their absolute positions can be used to gauge the dominant phonon frequency propagating across the crystal, while the caustic width gives a measurement of the phonon source size.*

Figure 16 shows a schematic of the phonon-focusing caustics around the [100] propagation direction with three scans of interest marked. From previous phonon dispersion studies,[26] we know that the ST caustic sampled by scan 1 is relatively insensitive to dispersive shifts, while the ST caustic in scan 2 and the FT caustic in scan 3 are quite sensitive to dispersive shifts. Figure 17 displays experimental images of this spatial pattern taken at two different times. Figure 17(a) is taken by sampling the phonon signal 900 ns after the laser pulse with a 200-ns gate and includes the ballistic arrival ($t_b = 940$ ns). Figure 17(b) samples the phonon signal 1900 ns after the laser pulse (again with a 200-ns gate) in the tail of the signal. *From the sharp caustics in Fig. 17(b), it is clear that the tail signal in this experiment is due to ballistic phonons from a delayed source emission, rather than diffusive phonons.*

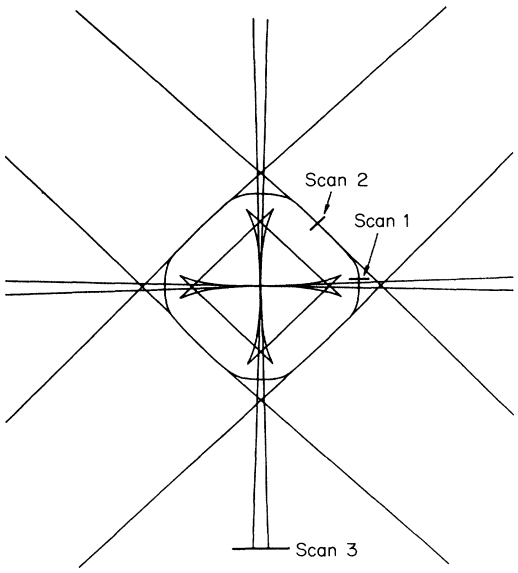

FIG. 16. Schematic of the phonon-focusing caustics around the [100] propagation direction in Si, indicating three spatial scans which will be studied in detail.

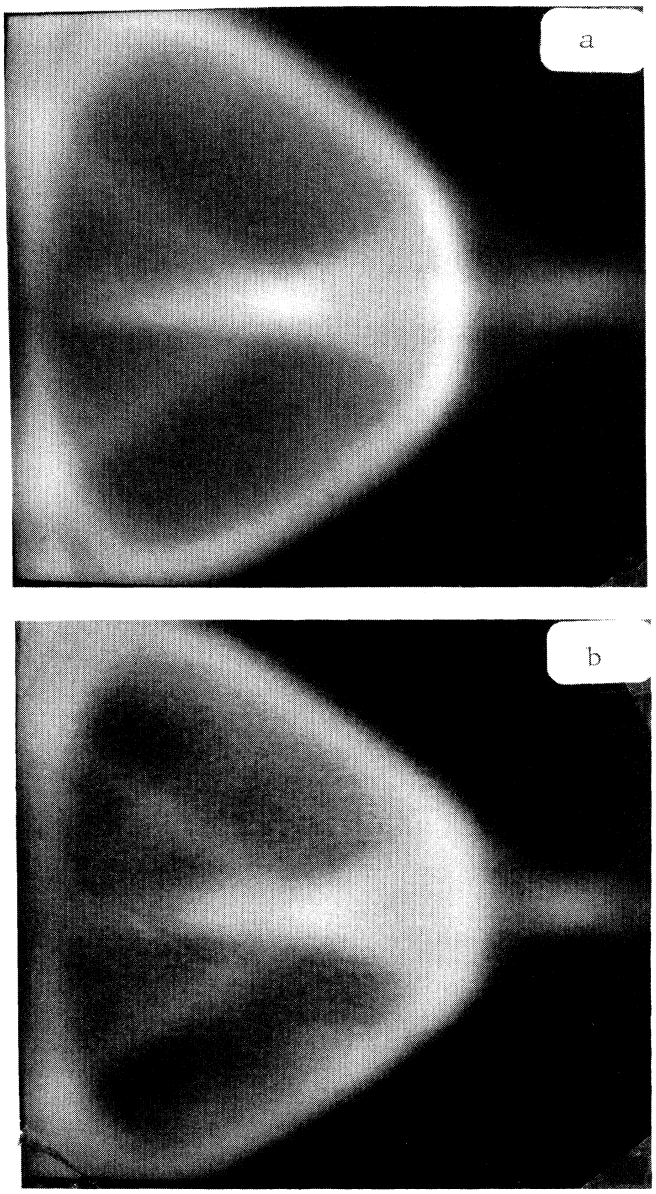

FIG. 17. Phonon images taken around the [100] propagation direction with a 200-ns gate which is (a) 900 ns and (b) 1900 ns after the laser pulse (the ballistic time is 960 ns). Note that the signal averaging is longer for image (b). The relative intensities can be estimated from the time traces of Fig. 15.

This conclusion is supported by observations of a long tail in the spatially filtered signal, as shown in Figs. 18(a) and 18(b), present only at higher powers. This delayed ballistic signal exhibits a distinct "cutoff time," which ranges from less than 1 to about 2 μs after the ballistic arrival time as the power density is increased [Fig. 18(c)]. The cutoff time may correspond to the disappearance of the bubble, but time-resolved optical-imaging experiments are required to verify this hypothesis. The cutoff times are roughly two orders of magnitude longer than predicted for a phonon hot spot, in Ref. 22.

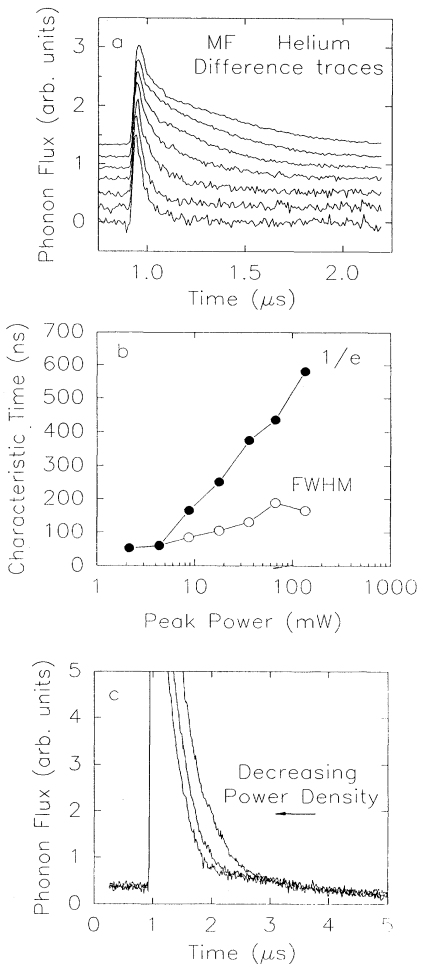

FIG. 18. Time trace differences from spatial filtering of the ST caustic signal (scan 2 in Fig. 16). The data shown were taken with a fixed excitation area of 1400 μm^2 while peak incident power is varied from 553 to 2.2 mW, top to bottom, and are normalized to the same peak height for ease of comparison. The tail of these ballistic-only time traces decreases with decreasing power density, indicating a changing source lifetime, influenced by helium-bubble formation. (b) Characteristic times for the phonon source, as indicated by the full width at half maximum of the difference-trace peaks and the $1/e$ time for the signal decay. (c) An enlargement of three time traces from (a) showing evidence for a cutoff time of the phonon signal which increases as power density is increased.

Careful study of the two images in Fig. 17 reveals that the phonon-focusing caustics have shifted noticeably in the 1-μs interval between them. These shifts are quantified in Fig. 19, which graphs the spatial positions of the peak in the ST caustic at scans 1 and 2 in Fig. 16. We see that the shifts in the caustic at scan 1 are constant within the error of the measurement. However, the caustic at scan 2 shows a dramatic displacement over time, corresponding to a shift in the detected phonon frequencies.

Figure 20 examines the temporal changes in the FT ridge (scan 3 in Fig. 16). Figure 20(a) is a series of scans across the ridge at different times, revealing a dramatic narrowing of the FT ridge (i.e., the two caustic peaks move closer together with increasing time). These shifts are quantified in Fig. 20(b). Figure 20(c) plots the phonon frequency corresponding to the angular separation of the two caustic peaks. (Details for the specialist: The conversion from angular widths to phonon frequencies relies upon a theoretical calculation of the ridge width versus frequency along the [110] direction made by Tamura, Shields, and Wolfe.[29] The data are scaled so that the full width at half maximum of the FT ridge at late times agrees with the calculated low-frequency peak separation, taking into account the difference in propagation angle in the experimental data, which is not along [110]. This conversion yields peak separations which correspond to a range of frequencies between 300 and 700 GHz. The vertical bars in Fig. 20(c) are an indication of the range of *detected* frequencies present in the caustic, as determined from the differences between the FWHM and peak separation [Fig. 20(b)].)

The changes in the peak separation of the FT ridge as a function of time indicate a temporal decrease in the dominant phonon frequency emitted by the source. The initial fast increase and the subsequent slow decrease in frequency are due to a fast rise in the temperature of the phonon source followed by slow cooling. Since the crystal transmits ballistically only phonons below about 1 THz, this method cannot determine the actual source temperature at early times. At $t \approx 2t_b \approx 2$ μs, however,

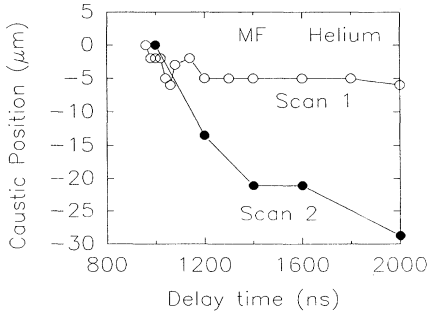

FIG 19. Shift in the caustic position as a function of time for two scans across the ST caustics, labeled in Fig. 16. The caustic shift in scan 2 indicates a decrease in the average phonon frequency emitted by the MF source. From previous phonon studies, the caustic in scan 1 is expected to be less sensitive to changes in phonon frequency than the caustic in scan 2.

we can say that the source has cooled to a temperature of $T \approx h(400\ \text{GHz})/2.8k_b \approx 7$ K. This slow drop in source temperature is also consistent with the decreasing width of the FT caustic for $t < 2$ μs shown in Fig. 21, indicating a narrowing frequency distribution in time. The width of the ST caustic, which is not expected to dispersively broaden, stays constant over time. This indicates that *although the source temperature is changing over time, the source size remains about 30 μm,* which may be limited by the laser spot size and bolometric resolution. These long localized-source lifetimes are not observed in the MF-vacuum case. We conclude that the helium bubble greatly lengthens the thermal relaxation time of the excited metal film. The properties of helium bubbles have been studied experimentally,[27,28] and it is known that the bubble dynamics depend upon the liquid-helium pressure at the crystal. In the present case the helium is confined in the small isolated space shown in Fig. 4 with just a small "leak" restricting flow to the helium bath. This configuration seems to extend the lifetime of the He bubble to more than 2 μs. Once the bubble is formed by the short excitation pulse, it slowly recondenses and the condensation energy heats the local surface region.

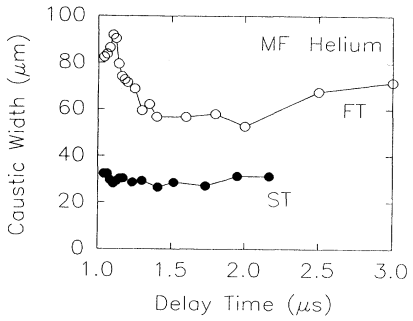

FIG. 21. Comparison of the change in two caustic widths (ST and FT as a function of time. The ST caustic width is relatively constant, indicating a constant source size, while the changes in the FT caustic width are a result of the changing frequency distribution of detected phonons, as in Fig. 20(c).

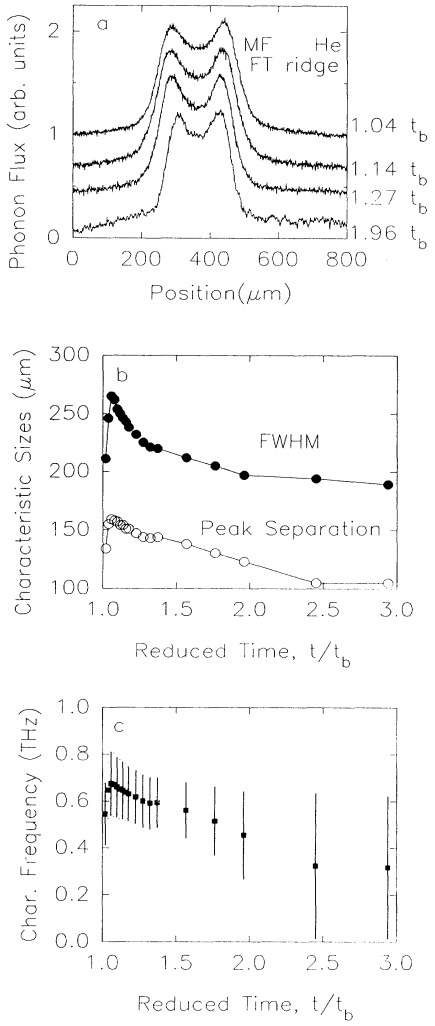

FIG. 20. (a) Line scans across the FT ridge (scan 3 in Fig. 16), taken at different times, relative to the ballistic time t_b. The signals are normalized to the same height and the traces at later times are collected with longer averaging time to increase their signal-to-noise ratio. (b) The characteristic sizes of the ridge, i.e., the peak separation and the full width at half maximum, are plotted as a function of the reduced time, t/t_b. (c) The characteristic sizes as a function of phonon frequency determined using a calculation by Tamura (Ref. 29). The vertical bars are an indication of the range of frequencies determined by the difference between the FWHM and the peak separation. These results indicate a very slow cooling of the MF, presumably associated with the existence of a helium bubble.

To summarize the results of our MF experiments, we find qualitative evidence that the phonons detected following photoexcitation of the copper film are consistent with a Planckian source model if phonon down conversion in the bulk is fully accounted for and possibly phonon reabsorption and down conversion in the cold regions of the metal film. With a vacuum interface, the fraction of ballistic signal decreases as the power density is raised, in stark contrast to the direct-photoexcitation case. When the copper film is in contact with the helium bath, a large increase in the integrated flux is observed as the power density is raised. This effect is attributed to the formation of a helium bubble which reduces the thermal losses from the copper film, thereby increasing the heat flux into the crystal. At high power, a localized heat source remains for up to 2 μs after the excitation pulse, interpreted as the bubble lifetime. The slow cooling of the source is observed by using the dispersive shifts in the phonon caustics.

VI. DIRECT PHOTOEXCITATION OF Si WITH A HELIUM INTERFACE

We saw in Fig. 6 that the presence of a helium interface greatly affects the shapes of the heat pulses produced by direct photoexcitation of silicon. At low powers, losses (predominantly of high-frequency phonons) to the helium bath almost completely suppress the long quasidiffusive tails of the heat pulse. At high powers, the

helium and vacuum interface conditions [Fig. 6(c)] show similar heat pulses, which is evidence for the formation of a new source of low-frequency phonons. There is still an unexplained anomaly associated with the condensed film in the "isolated surface" case [Fig. 6(b)].

As discovered in the metal-film experiments, the formation of a helium bubble at high excitation density has a great effect on the heat pulses. Direct evidence for the formation of a bubble in the DP case is contained in the experiment of Fig. 22, which is conducted with a long (700 ns) excitation pulse in order to increase the signal level at low absorbed power. The figure shows a power dependence of the heat-pulse intensity at a constant excitation area of 200 μm^2. [Notice that the lowest power density on this scale is (0.01 mW)/(200 μm^2)=0.05 W/mm^2, which is about two orders of magnitude below that of Fig. 9.] An approximately linear relation is seen except for the abrupt order-of-magnitude jump at 5 mW. Concurrent with this jump in intensity, an abrupt increase in the scattered laser light at the excitation point is observed, indicating that a helium bubble is formed. As discussed earlier, the formation of a gaseous bubble reduces the thermal contact to the superfluid helium bath, thus increasing the heat-pulse signal. The threshold power for the bubble formation depends on the focal spot size.

We now return to the short-pulse (10 ns) case and measure the intensity of the ballistic pulse at constant power but varying power density (i.e., by defocusing). In Fig. 23 these results are compared to the isolated surface case, replotted from Fig. 9. (The vacuum surface case is qualitatively similar). The relative intensity between the two experiments is not known, so we have arbitrarily set the intensities equal at the highest power density. The data show a much larger and more abrupt change in intensity for the helium-interface case. We attribute this enhancement to a change in the boundary condition concurrent with the formation of the localized heat source. (The helium bubble is visually confirmed at the power density where the abrupt increase in phonon signal is observed.) It seems probable that the formation of the localized source in the crystal, confining the thermal energy near the surface of the crystal, drives the formation of the bubble. If the localized source is viewed as a diffusive region for the phonons, then the diffusing phonons can be lost to the liquid or gas at the surface, producing a change in the form of the detected heat pulses. If it were not for the observed thresholds in the isolated interface data (also present in mechanically pumped vacuum data), it would be tempting to ascribe the helium bubble as the principal cause of a "hot spot." We see, however, that the situation is much more complicated—involving the dynamics of the helium as well as the phonon dynamics in the crystal.

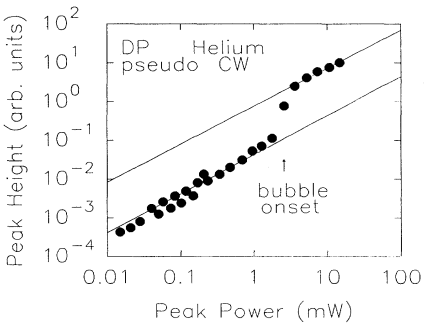

FIG. 22. Peak phonon signal intensity as a function of absorbed power with DP-helium excitation. These data are taken with a very long laser pulse (700 ns) and a correspondingly long boxcar gate (500 ns) in order to increase the total phonon signals at low power densities and a fixed laser spot size (excitation area 200 μm^2). The jump in intensity at 2.5 mW is correlated with the formation of a helium bubble at the excitation point. Once the bubble forms, phonon losses into the helium bath decrease.

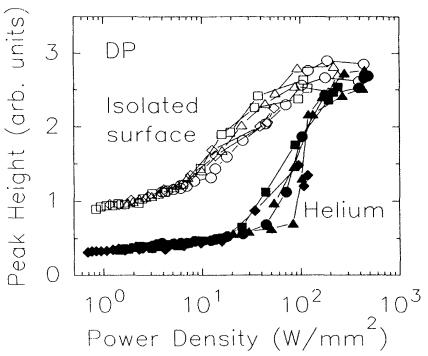

FIG. 23. Comparison of the defocusing data for the isolated surface and helium interfaces under direct photoexcitation, showing the change in peak height as a function of absorbed power density for four different peak powers, ranging from 80 to 660 mW. The data show a much larger and more abrupt change in intensity for the helium case, coincident with the formation of a helium bubble.

VII. SUMMARY AND DISCUSSION

While there are some intriguing unsolved mysteries about the nonequilibrium phonons in photoexcited Si, our experiments have brought into clearer focus a number of aspects of this system. In the first place, the contact of the excitation surface with a helium bath masks the intrinsic anharmonic-decay processes by providing a loss mechanism for high-frequency (diffusive) phonons. When the excitation surface is isolated by a vacuum and the excitation density is sufficiently low, the predicted anharmonic and elastic-scattering processes are manifest in the shape of the detected heat pulses (e.g., Fig. 4), characteristic of a "quasidiffusive" propagation. In contrast, the heat pulses produced by moderate photoexcitation of a copper film evaporated on the Si surface are characterized by low-frequency ballistic propagation, due to the effectiveness of the metal film in producing a thermalized, perhaps Planckian, distribution of phonons.

As the power density is increased in the helium-interface cases, a bubble of vaporized He gas is formed at the excitation point, and this local change in the boundary condition has large effects on the shape of the detect-

ed heat pulses. In general, the detected heat flux is greatly enhanced by the bubble formation—by factors of 3–10—depending on the conditions (e.g., pulse length). For 10-nJ excitation power, the bubble apparently has a lifetime of several microseconds, which, in the case of metal-film excitation, causes the metal film to cool slowly. (The calculated relaxation time of a heated metal film contacting a cold substrate and superfluid helium is only about a nanosecond.) To examine the effect of the helium on nonequilibrium crystal phonons, concurrent optical experiments which time resolve the bubble dynamics are required, such as those conducted by Greenstein and Wolfe.[27]

In the case of directly photoexcited silicon without liquid helium at the excitation interface, a clear threshold has been observed for the formation of a localized source of low-frequency phonons. In other words, at sufficient power density, the rather slow anharmonic-decay process [Eq. (1)] is not limiting the production of low-frequency phonons which propagate ballistically to the detector. If not, then what is producing the preponderance of low-frequency phonons? A crude calculation shows that the formation threshold for the localized source is three or four orders of magnitude lower than predicted for a phonon "hot spot" which relies only on phonon-phonon interactions. In addition, the lifetime of the localized source is one or two orders of magnitude longer than the predicted "hot-spot" lifetime.

We postulate that photoexcited carriers are playing a critical role in the formation of the localized phonon source in DP silicon. While a direct link to the carriers has not yet been established, we point to a variety of supporting evidence. At low temperatures and excitation densities, the electron-hole pairs form excitons, which have measured lifetimes of a few microseconds, limited by nonradiative recombination at impurities or defects. Such recombination produces nonequilibrium phonons, presumably high-frequency phonons, which would propagate quasidiffusively. However, it is well known that in low-temperature Si at moderate excitation levels, electron-hole droplets[30] with an *e-h* pair density of 3.3×10^{18} cm^{-3} and a fraction of a micrometer radius are formed, either by condensation of excitons, or direct formation from the photoproduced plasma at the excitation surface. Photoluminescence imaging experiments[31,32] have shown that there are strong interactions between nonequilibrium phonons and electron-hole droplets. Phonons produced by carrier thermalization and recombination are easily absorbed by droplets and, by transferring their momentum, the phonons push the droplets away from the excitation surface.[32,33]

The droplets themselves are also a source of nonequilibrium phonons. In silicon, recombination of an electron-hole pair in an electron-hole droplet is predominantly a nonradiative (Auger) process, in which the band-gap energy of the annihilating pair is converted to kinetic energy of another carrier in the droplet. This kinetic energy is converted to heat as the hot carrier relaxes by scattering and phonon emission. A recent calculation by Esipov, Msall, and Wolfe[34] attempts to estimate the frequency distribution of phonons emitted by this thermalization process. At first thought, one might suspect that the hot carriers would produce a number of LO phonons, which down convert to acoustic phonons and decay. As in the quasidiffusion process described earlier, this would not produce a rich source of low-frequency phonons. However, at the carrier density present in an electron-hole droplet, it becomes likely that the hot carrier will quickly transfer its kinetic energy to other carriers, thereby heating up the droplet as a whole. It turns out that the phonon spectrum produced by this process is rich in subterahertz phonons, just as in the case of a metal.

In view of this it is tempting to conclude that the cloud of droplets is itself the localized source of low-frequency phonons observed in our experiments. Several known properties of the droplets seem to support this idea. First, we have observed photoluminescence from droplets in these crystals under similar excitation conditions. Second, the lifetime of electron-hole droplets in Si is about 140 ns, which is very close to the measured lifetime of the phonon source in Fig. 10. Third, the cloud of droplets is known to be fairly localized: (1) In cw excitation experiments by Tamor and Wolfe,[33] the cloud size ranges from about 30 to 100 μm for single-line Ar^+-laser excitation, as in the present experiments. The cloud sizes of Tamor are remarkably similar to the phonon-source-size data reported by Shields and Wolfe,[16] although one must realize that the latter experiments were conducted with pulsed excitation; (2) time-resolved imaging[31] of the cloud following 10 ns pulsed excitation with 430 nJ pulse energy at 10 K shows an expanding cloud with a final radius of about 175 μm. The expansion mechanism is attributed to the "phonon-wind" pressure from nonequilibrium phonons. The cloud radius is expected to be considerably smaller at the typical 10-nJ excitation level in the present experiments.

The question of whether the droplets (and early plasma) are acting as the down-conversion medium for high-frequency phonons created by initial carrier thermalization events or are themselves a principal source of low-frequency phonons must be answered by further experimentation. The source lifetime data of Fig. 10 and the theory of Esipov favor the latter scenario.

A number of other experiments come to mind. First, it is important to make detailed measurements of the *relative* intensities of heat pulses with vacuum and helium interfaces, in order to account for the losses. Second, the threshold power for the formation of the localized source can be compared to the threshold for electron-hole droplet formation. It is also possible to change the properties (e.g., *e-h* density, threshold, lifetime) of the droplets by applying stress to the crystal, which has little effect on the acoustic properties. Finally, the techniques introduced in the present paper can be applied to other semiconductors (e.g., Ge, GaAs), which have widely different excitonic properties from Si. For example, the exciton lifetimes in GaAs are only about 1 ns, due to its direct semiconducting gap, and no droplets have been observed. In contrast, droplets in Ge have about 300 times longer lifetime than those in Si, making them a much weaker phonon source.

One thing seems clear from the current data: the frequency and spatial distributions of nonequilibrium acoustic phonons produced by direct photoexcitation of a semiconductor is a problem rich in complex interactions, and not likely to be solved by a "generic" model. We believe that the present systematic studies have exposed most of the relevant processes for silicon and identify the paths to understanding acoustic-phonon propagation for other crystals and excitation conditions.

ACKNOWLEDGMENTS

This work was supported by the National Science Foundation under the Materials Research Laboratory Grant No. DMR-89-20538. M.C. was supported by a NSF REU grant. The high-purity Si crystal used for these experiments was obtained from Siemens and is characterized by $N_A - N_D \approx 10^{12}$ cm^{-3}. We acknowledge useful discussions with S. Esipov.

[1]See, for example, *Phonons 89,* edited by S. Hunklinger, W. Ludwig, and G. Weiss (World Scientific, Singapore, 1990).

[2]R. J. VonGutfield, in *Physical Acoustics,* edited by R. P. Mason (Academic, New York, 1968), Vol. 5.

[3]H. Kinder, in *Nonequilibrium Phonon Dynamics,* edited by W. E. Bron (Plenum, New York, 1965).

[4]G. A. Northrop and J. P. Wolfe, in *Nonequilibrium Phonon Dynamics,* edited by W. E. Bron (Plenum, New York, 1965).

[5]J. A. Shields, S. Tamura, and J. P. Wolfe, Phys. Rev. B **43**, 4966 (1991).

[6]Tamura and Maris have performed calculations of the anharmonic-decay rates, including anisotropy. See H. J. Maris and S. Tamura, Phys. Rev. B **47**, 727 (1993).

[7]See, for example, B. Sadoulet, B. Cabrera, H. J. Maris, and J. P. Wolfe, in *Phonons 89,* Ref. 1, and references cited therein.

[8]H. J. Maris, in *Phonon Scattering in Condensed Matter V,* edited by A. C. Anderson and J. P. Wolfe (Springer-Verlag, Berlin, 1989).

[9]S. Tamura, Phys. Rev. B **31**, 2574 (1985).

[10]S. Tamura, Phys. Rev. B **27**, 858 (1983).

[11]D. V. Kazakovtsev and I. B. Levinson, Phys. Status Solidi B, **96**, 117 (1979).

[12]Y. B. Levinson, in *Nonequilibrium Phonons in Nonmetallic Crystals,* edited by W. Eisenmenger and A. A. Kaplyanski (North-Holland, Amsterdam, 1986), p. 91.

[13]W. E. Bron, Y. B. Levinson, and J. M. O'Connor, Phys. Rev. Lett. **49**, 209 (1982).

[14]G. A. Northrop and J. P. Wolfe, in *Phonon Scattering in Condensed Matter IV,* edited by W. Eisenmenger, K. Lassmann, and S. Döttinger (Springer-Verlag, Berlin, 1984). See also Ref. 19.

[15]H. J. Maris, Phys. Rev. B **41**, 9736 (1990).

[16]J. A. Shields and J. P. Wolfe, Z. Phys. B **75**, 11 (1989).

[17]Y. B. Levinson, in *Phonons 89,* edited by S. Hunklinger, W. Ludwig, and G. Weiss (World Scientific, Singapore, 1990).

[18]A. F. G. Wyatt, in *Nonequilibrium Superconductors, Phonons and Kapitza Boundaries,* edited by K. E. Grey (Plenum, New York, 1981).

[19]B. A. Danil'chenko, D. V. Kazakovtsev, and M. I. Slutskii [Phys. Lett. A **138**, 77 (1989)] have previously reported the dependence of heat pulses in GaAs on excitation density. In contrast to our results, they found power-dependent changes in the heat pulse which suggested the formation of a phonon hot spot in GaAs at high excitation densities. We point out that the carrier lifetime in GaAs is quite short (about 1 ns), so that the energy evolution of the phonon distribution after a few ns takes place in the absence of phonon-carrier scattering.

[20]M. Greenstein, M. A. Tamor, and J. P. Wolfe, Phys. Rev. B **26**, 5604 (1982).

[21]C. Hensel and R. C. Dynes, Phys. Rev. Lett. **39**, 969 (1977).

[22]D. V. Kazakovtsev and Y. B. Levinson, Zh. Eksp. Teor. Fiz. **88**, 2228 (1985) [Sov. Phys. JETP **61**, 1318 (1985)].

[23]N. M. Guseinov and G. S. Orudzhev, Fiz. Tverd. Tela (Leningrad) **29**, 2269 (1987) [Sov. Phys. Solid State **29**, 1308 (1987)].

[24]G. Müller and O. Weis, Z. Phys. B **80**, 15 (1990).

[25]O. Weis, Z. Angew. Phys. **26**, 325 (1969).

[26]S. E. Hebboul and J. P. Wolfe, Phys. Rev. B **34**, 3948 (1986).

[27]M. Greenstein and J. P. Wolfe, J. Phys. (Paris) Colloq. **XX**, C6-274 (1981).

[28]V. A. Tsvetkov, A. S. Alekseev, M. M. Bonch-Osmolovskii, T. I. Galkina, N. V. Zamkovets, and N. N. Sibel'din, Pis'ma Zh. Eksp. Teor. Fiz. **42**, 272 (1985) [JETP Lett. **42**, 335 (1985)].

[29]S. Tamura, J. A. Shields, and J. P. Wolfe, Phys. Rev. B **44**, 3001 (1991).

[30]T. M. Rice, in *Solid State Physics: Advances in Research and Applications,* edited by H. Ehrenreich, F. Seitz, and D. Turnbull (Academic, New York, 1977), Vol. 32, p. 1; J. C. Hensel, T. G. Phillips, and G. A. Thomas, *ibid.*, p. 88.

[31]F. M. Steranka, Phys. Rev. B **34**, 1014 (1986).

[32]J. P. Wolfe, J. Lumin. **30**, 82 (1982).

[33]M. A. Tamor and J. P. Wolfe, Phys. Rev. B **21**, 739 (1980).

[34]S. Esipov, M. Msall, and J. P. Wolfe, Phys. Rev. B (to be published).

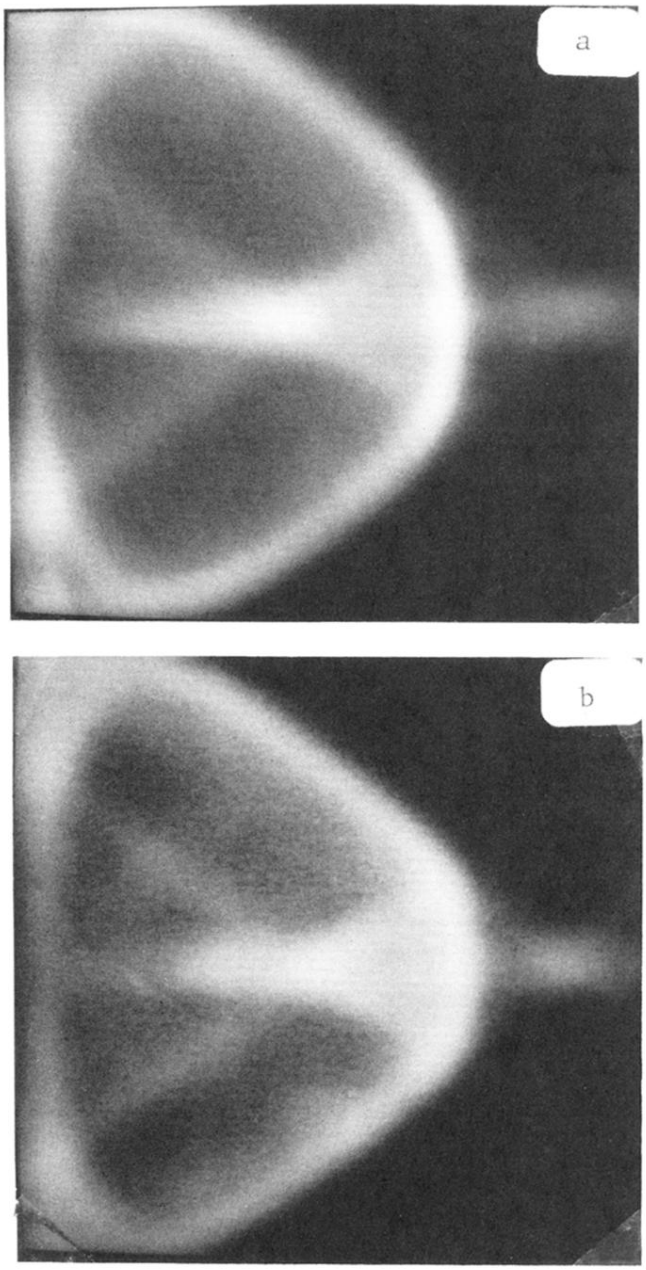

FIG. 17. Phonon images taken around the [100] propagation direction with a 200-ns gate which is (a) 900 ns and (b) 1900 ns after the laser pulse (the ballistic time is 960 ns). Note that the signal averaging is longer for image (b). The relative intensities can be estimated from the time traces of Fig. 15.

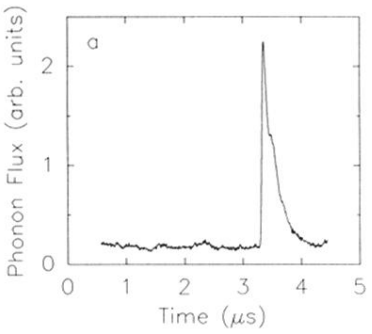

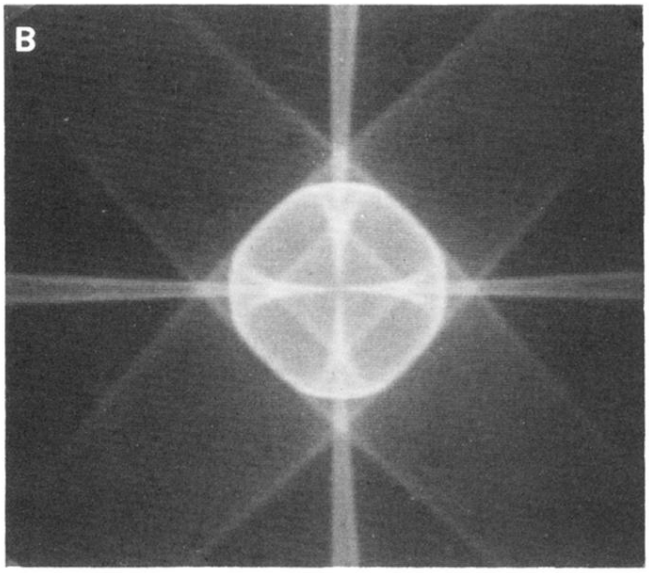

FIG. 3. (a) Intensity of the phonon signal vs time in photoexcited silicon at $T=1.8$ K. The propagation direction is along a slow transverse (ST) caustic which is 7° from [001] in the 010 horizontal plane. The onset of the ballistic signal at $t=3.2$ μs indicates significant ST ballistic signal. The longitudinal pulse is not observed due to phonon focusing. The central caustic structure is referred to as the "ST box" (Ref. 16). (b) High-resolution phonon image of silicon with direct photoexcitation. The center of the image corresponds to the [001] propagation direction. The width of the image is about 43° left to right.